Acta of Bioengineering and Biomechanics
Vol. 20, No. 2, 2018

Original paper
DOI: 10.5277/ABB-01131-2018-02

One step 3D printing of surface functionalized composite scaffolds for tissue engineering applications

MARCIN KOTLARZ[1], RAINER JORDAN[2], ERIK WEGENER[2], PIOTR DOBRZYŃSKI[3], JÖRG NEUNZEHN[4], ALBENA LEDERER[5], CORNELIA WOLF-BRANDSTETTER[4], ELZBIETA PAMULA[1], DIETER SCHARNWEBER[4]*

[1] AGH University of Science and Technology,
Faculty of Materials Science and Ceramics, Krakow, Poland.
[2] Technische Universität Dresden, Faculty of Chemistry and Food Chemistry,
Chair of Macromolecular Chemistry, Dresden, Germany.
[3] Center of Polymer and Carbon Materials, Polish Academy of Sciences, Zabrze, Poland.
[4] Technische Universität Dresden, Institut für Werkstoffwissenschaft,
Max-Bergmann-Zentrum für Biomaterialien, Dresden, Germany.
[5] Leibniz-Institut für Polymerforschung Dresden e.V., Institut für Makromolekulare Chemie,
Polymer Separation Group, Dresden and Technische Universität Dresden, Dresden, Germany.

Purpose: A successful approach widely used in materials science to adapt approved materials to specific applications is to design their surface properties. A main challenge in this area is the development of processing routes enabling for a simple but efficient surface design of complex shaped geometries. Against this background, this work aimed at the implementation of self-assembly principles for surface functionalization of 3D-printed poly(lactic-co-glycolic acid) (PLGA)-based constructs with macro- and microporous geometries via precision extruding deposition.

Methods: Three-component melts from PLGA, $CaCO_3$ and amphiphilic polymers (poly(2-oxazoline) block copolymer) were printed and their bulk and surface properties were studied.

Results: Melts with up to 30 mass % of $CaCO_3$ could be successfully printed with homogeneously distributed mineral particles. PLGA degradation during the printing process was temperature and time dependent: the molecular weight reached 10 to 15% of the initial values after ca. 120 min of heat exposure. Filament surfaces from melts containing $CaCO_3$ show an increasing microroughness along with increasing $CaCO_3$ content. Surface roughness and amphiphilic polymer content improve scaffold wettability with both factors showing synergistic effects. The $CaCO_3$ content of the melts affected the inner filament structure during *in vitro* degradation in PBS, resulting in a homogeneous mineral particle-associated microporosity for mineral contents of 20 mass % and above.

Conclusions: These results provide novel insights into the behavior of three-component melts from PLGA, $CaCO_3$ and amphiphilic polymers during precision extruding deposition and show for the first time that self-assembly processes can be used to tailor scaffolds surface properties under such processing conditions.

Key words: *3D printing, PLGA, calcium carbonate, amphiphilic poly(2-oxazoline), degradation, surface properties*

1. Introduction

Saturated poly(α-hydroxy acids) such as polylactide (PLA), polyglycolide (PGA) and poly(lactide-co-glycolide) (PLGA) are synthetic biodegradable polymers widely used for biomedical applications [4]. Major advantages are their highly controlled degradation and excellent reproducible mechanical and physical properties. These can be tuned by the molecular weight and for PLGA, additionally by the copolymer ratio and chain structure [14]. In applications designed

* Corresponding author: Dieter Scharnweber, TU Dresden, Max Bergmann Center of Biomaterials, Budapester Straße 27, 01069 Dresden, Germany. Phone: +49 35146339379, e-mail: Dieter.Scharnweber@tu-dresden.de

Received: April 11th, 2018
Accepted for publication: June 11th, 2018

for bone reconstruction PLGA is often combined with ceramic materials such as bioglass or calcium phosphate phases (CPP) [22]. Apart from improving the osteoconductivity and the mechanical properties, these components additionally reduce negative effects of the autocatalytic bulk degradation by quenching acidic degradation products [27]. Besides, a number of techniques have been used for surface functionalization of PLGA reaching from oxygen plasma treatment to introduce negatively charged groups [2] to covalent coupling of peptide sequences [8]. For the plasma treatment, an improved mineralization in simulated body fluid as well as enhanced adhesion and proliferation of osteoblast-like cells has been shown [17].

In previous work we have applied surface modification to PLGA structures using main components of the organic extracellular matrix (ECM) of soft and hard tissues, such as collagen type I and glycosaminoglycans [20], like chondroitin sulphate, dermatan sulphate, and hyaluronic acid for coating in order to mimic the native environment of cells [18], [24], [25]. These different approaches demonstrate the high potential of PLGA surface modifications to improve the biological response to PLGA-based implants and scaffolds.

For 3D-printing of polymeric materials, in recent years a number of technologies such as, e.g., stereolithography [13], selective laser sintering [5], and fused deposition modelling (FDM) [11] have been utilized. FDM as technology applied in this work has already been used to prepare scaffolds from PLGA [16], [29]. In combination with various CPP and bioglass, this process can be adapted to the specific defect geometry presenting a defined pore structure [9], [22]. FDM of a 50:50 PLGA copolymer with a processing temperature of 170 °C was found to decrease the average molecular weight from approximately 100 to 65 kDa [29]. Lowering the processing temperatures for PLGA with a similar molecular weight to 110 °C was found to improve compressive modulus [16].

Previous work in our group has applied the FDM route to process poly(ε-caprolactone) (PCL) together with mineral phases (hydroxyapatite and/or $CaCO_3$) (6). For up to 50 mass % of $CaCO_3$ the compound material could be printed appropriately with the mineral particles evenly distributed in the polymer matrix [6]. The use of $CaCO_3$ instead of a less soluble CPP, such as hydroxyapatite, may be beneficial. The more rapid dissolution of $CaCO_3$ will result in an improved buffering of acidic polymer degradation products and is expected to generate a microporosity of the 3D-printed constructs to improve the biological interaction between the scaffold and the host tissue [15].

The aim of this study was to perform FDM processing of two- and three-component melts from PLGA, $CaCO_3$ and an amphiphilic polymer and to study their bulk and surface properties. Our working hypothesis was that the conditions during FDM processing allow for the regio-selective self-organization of amphiphilic molecules at the interface between the hydrophobic PLGA and the hydrophilic environment, as realized by the inner surface of the printing system and the atmospheric environment. Additionally, it was of special interest whether the combination of amphiphilic molecules with $CaCO_3$ results in synergistic effects regarding the wetting behavior of the resulting scaffold surfaces and to follow the formation of microporosity during degradation.

2. Materials and methods

Materials

Poly(L-lactide-co-glycolide) (PLGA) (85:15, molar ratio of L-lactide to glycolide) (Center of Polymer and Carbon Materials, Polish Academy of Sciences, Zabrze, Poland), Calcium carbonate ($CaCO_3$) with a specific surface area of 3 m^2/g (Schaefer Kalk, Germany), amphiphilic poly(2-oxazoline) blockcopolymer Me-P[NonOx11-b-MeOx35]-Pip abbreviated as POx (Fig. 1), synthesized by living cationic ring-opening polymerization by the Chair of Macromolecular Chemistry, Technische Universität Dresden, Germany, were used in the experiments.

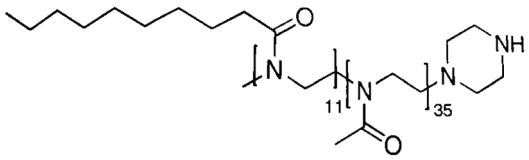

Fig. 1. Structural formula of poly(2-oxazolines)-copolymer Me-P[NonOx11-b-MeOx35]-Pip

Scaffold preparation

Computer models of the scaffolds were created in the BioCAD software (regenHU, Switzerland). Scaffolds were fabricated using the HM300H, a high temperature printing head connected to a 3D Discovery® system (regenHU, Switzerland).

For scaffolds fabrication the following parameters have been modified prior printing process: tank temperature T_t (°C), extruder barrier screw temperature T_e (°C), the extruder feed rate V_e (revs/m) which is relative to the speed of the instrument's

movement, the printing head feed rate V_d (mm/s), the cartridge pressure p (MPa), the distance between strains Δx (mm) and the heating plate temperature T_p (°C). The following range of the printing parameters have been investigated T_t: 191 – 155 °C, T_e: 186 – 150 °C, V_e: 14 – 10 revs/m, V_d: 5 – 3 mm/s, p = 0.6 MPa, Δx = 0.6 mm. The diameter used needle was 0.26 mm. The scaffolds have been printed on a glass slide fixed with a Kapton® tape on a heating plate with a surface temperature T_p = 40 – 45 °C.

Respective material systems were firstly mixed together, put into the tank and melted directly inside the tank, occasionally blended with a spatula to gain a homogenous melt. After melting, the printing process was started. The material was pressed to the barrier screw by air pressure and thus the filament was released through the needle (Fig. 2). The printing process aimed to produce geometries with regular and controlled macroscopic pores.

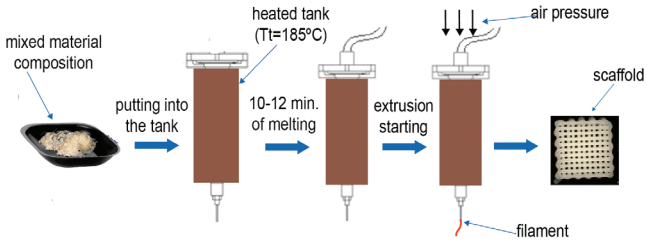

Fig. 2. Schematic melting and extrusion procedure

The following melt systems have been evaluated:
(1) PLGA,
(2) PLGA with 1 mass % POx,
(3) PLGA with 10 mass % $CaCO_3$,
(4) PLGA with 10 mass % $CaCO_3$ and 1 mass % POx,
(5) PLGA with 20 mass % $CaCO_3$,
(6) PLGA with 30 mass % $CaCO_3$.

Sample geometries utilized in the different experiments were:
(1) scaffolds 8 × 8 × 2 mm for SEM,
(2) scaffolds 6 × 6 × 6 mm for degradation investigations,
(3) dense samples 8 × 8 mm with two printed layers for water contact angle measurements.

Gel permeation chromatography (GPC)

Gel permeation chromatography (GPC) was used to determine the molecular weight and polydispersity of the 3D-printed porous material. The GPC measurements were performed using an HPLC system consisting of a pump and refractive index detector (1100 series, Agilent Technologies). The samples were dissolved in chloroform and filtered through a 0.2-µm syringe filter prior to separation performed on a PLgel MIXED-B-LS column (300 mm × 7.5 mm) at a flow rate of 1 ml/min and with chloroform as eluent. Molecular weights were calculated based on polystyrene standards.

Optical microscopy and Scanning Electron Microscopy (SEM)

Porosity and morphology of the scaffolds were studied with the use of an optical microscope KEYENCE VHX-1000D. SEM analysis was performed using a ZEISS DSM 982 Gemini instrument. For structural evaluation of scaffolds morphology, images were obtained using the backscattering electron mode (BSE) and secondary electron detector mode (SE) at 15 kV and 3 kV acceleration voltage, respectively. Prior to SEM investigations, samples were coated with a few nanometers of carbon.

Water contact angle measurements

Wettability of printed substrate surfaces was studied on 8 × 8 mm samples which consisted of 2 layers of densely printed material with direct fusion of the neighbouring strains. Water contact angles were measured applying the static sessile drop (8 µl) technique with a contact angle goniometer (Data Physics OCA 15).

Degradation investigations

In vitro degradation of scaffolds was performed in phosphate buffered saline (PBS) at pH of 7.4 at 37 °C. Scaffolds were placed in a 15 ml Falcon tubes (Greiner bio-one) and 10 ml of PBS was added.

Statistics

For statistical analysis the Shapiro–Wilk test was performed to test the assumption of normality followed by one-way ANOVA and a Holm–Sidak test. Significant differences were assumed at $p < 0.05$*, $p < 0.001$**.

3. Results

3.1. Influence of printing parameters on scaffold geometry

Within this set of experiments the influence of different printing parameters on the geometrical features

of the scaffolds, such as strain thickness and pore size has been studied for different melt compositions. Figure 3 shows exemplarily for the melt system PLGA with 10 mass % $CaCO_3$ the influence of the printing head feed rate and the extruder feed rate on the average filament width and the corresponding average pore size.

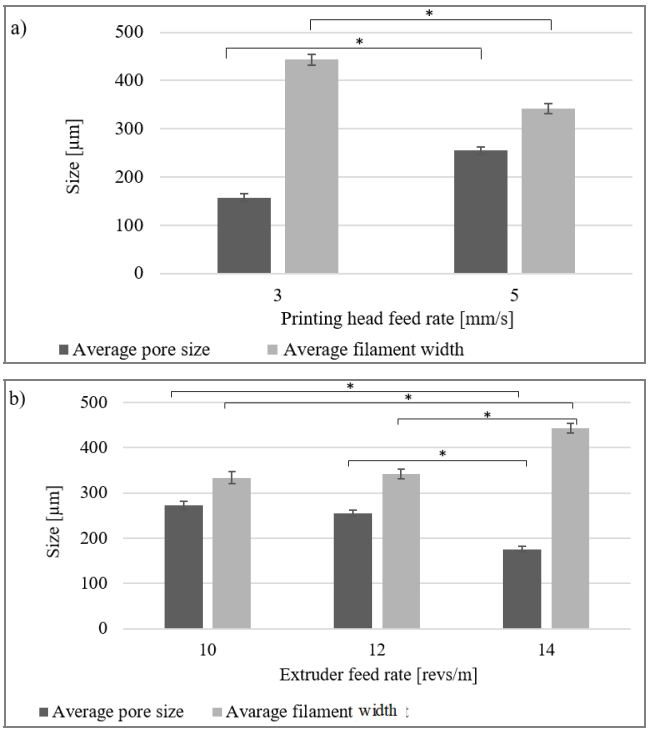

Fig. 3. Effect of printing parameters on scaffold geometry for PLGA scaffolds with 10 mass % of $CaCO_3$: Pore size and filament width for variable printing head feed rates (a) and for variable extruder feed rates (b). Constant printing parameters in (a): T_t = 160 ºC, T_e = 155 ºC, V_e = 12 revs/m; in (b): T_t = 160 ºC, T_e = 155 ºC, V_d = 5 mm/s

Whereas an increasing printing head feed rate results in a significantly decreasing filament width, and consequently, in an increasing pore size, the effect of an increasing extruder feed rate is opposite, i.e., it results in a significant increase in the filament width associated with a decreasing pore size.

In general, for the printing process, the tank temperature T_t and the extruder barrier screw temperature T_e have to be close to each other. Furthermore, the printer's manufacturer recommends that T_t should be slightly higher than T_e. Based on this recommendation, all experiments have been performed with a constant ΔT of 5 K between T_t and T_e. Typical results of experiments studying the effect of the tank temperature on the resulting scaffold geometries are displayed for the melt system PLGA with 20 mass % of $CaCO_3$ in Fig. 4. A decrease in printing temperature results in a significant reduction of the strain width and a corresponding bigger pore size.

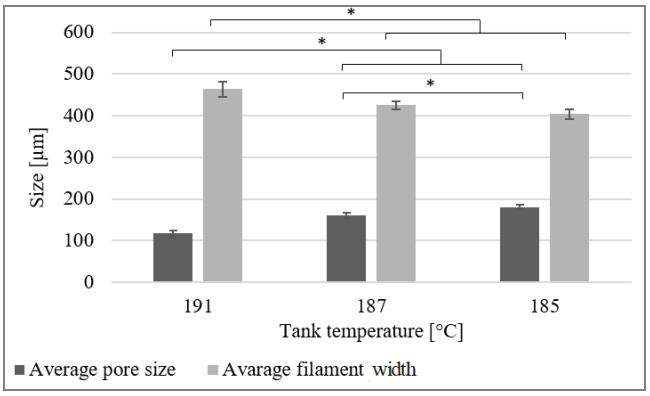

Fig. 4. Effect of printing parameters on scaffold geometry for PLGA scaffolds with 20 mass % of $CaCO_3$: Pore size and filament width for variable printer tank temperatures (extruder temperature 5 K below tank temperature). Constant printing parameters in: V_e = 10 revs/m, V_d = 3 mm/s. Analysis based on 60 independent measurements each from three scaffolds per batch

Resulting from this set of investigations the following parameters were used as standard conditions for all following experiments for all melt systems:

- starting T_t = 185 °C,
- starting T_e = 180 °C,
- V_e = 12 revs/m,
- V_d = 5 mm/s.

The melting time before starting printing was 10–12 min. T_t and T_e were constantly decreased due to PLGA degradation (as shown in chapter 3.2) to maintain constant pore size and filament width of fabricated scaffolds.

3.2. Molar mass evaluation

PLGA degradation during the printing process has been studied by measurement of the number-average molecular weight (M_n) and the weight average molecular weight (M_w). Both parameters and the dispersity (M_w/M_n), are plotted as a function of the printing temperature T_t in Fig. 5. As a second x-axis printing time is included.

The values before printing in the diagrams represent the starting material with M_w = 328.267 ± 5.200 g/mol, M_n = 109.000 ± 6.239 g/mol and a resulting polydispersity of 3.0 ± 0.2. During preparation of the melt in the printer (melting time 10–12 min) both M_w and M_n decrease significantly to values of ~120.000 ± 650 g/mol and ~24.000 ± 300 g/mol, respectively. Continuous printing over a time span of 120 min results in further

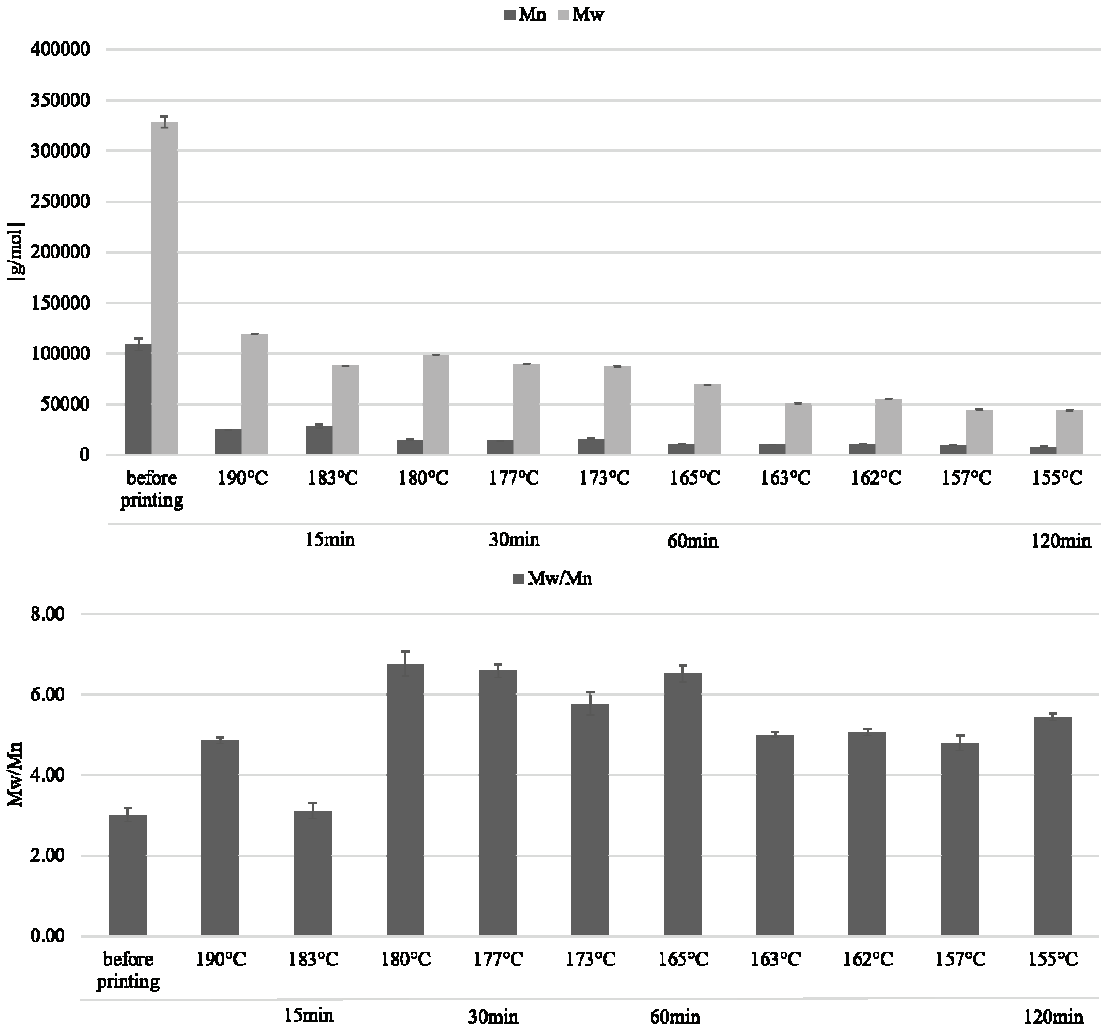

Fig. 5. Molar weight evaluation with prolonged storage time in the tank and constantly decreased printing temperature T_t. (a) number average molecular weight (M_n) and weight average molecular weight (M_w), (b) Dispersity (M_w/M_n)

decrease of both values to ~43.000 ± 550 g/mol for M_w and ~8.000 ± 200 g/mol for M_n. The dispersity of the PLGA is increased during the initial melting to 4.8 ± 0.1, followed by a further increase up to 6.8 ± 0.3 in maximum after about 15 min printing time. Afterwards the polydispersity stabilizes in the range between 5.0 and 6.5. Selective measurements in the system PLGA + 10 mass % of $CaCO_3$ are consistent with the results for the pure PLGA system (data not shown).

3.3. Morphology of 3D scaffolds

Light microscopic images of printed scaffolds of varying composition are presented in Fig. 6, while corresponding SEM images are shown in Fig. 7.

Light microscopic images show transparent PLGA and PLGA + 1 mass % of POx filaments with the addition of POx resulting a slightly brownish colour.

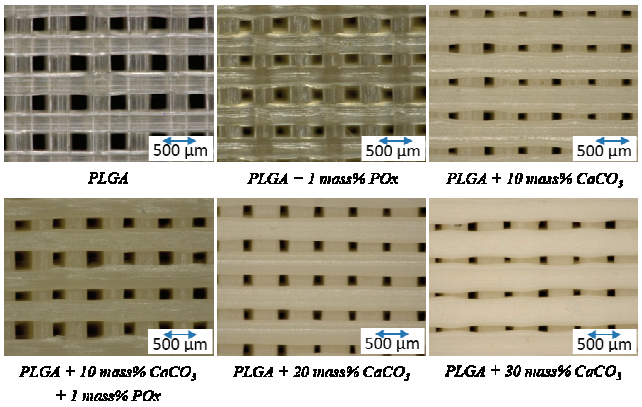

Fig. 6. Optical microscope images of printed scaffolds (100×)

An increasing amount of $CaCO_3$ in the filaments results in more milky structures with again a slightly brownish colour for the melt system with both, $CaCO_3$ and POx. Increasing $CaCO_3$ content in the melt system additionally results in the thicker filaments and

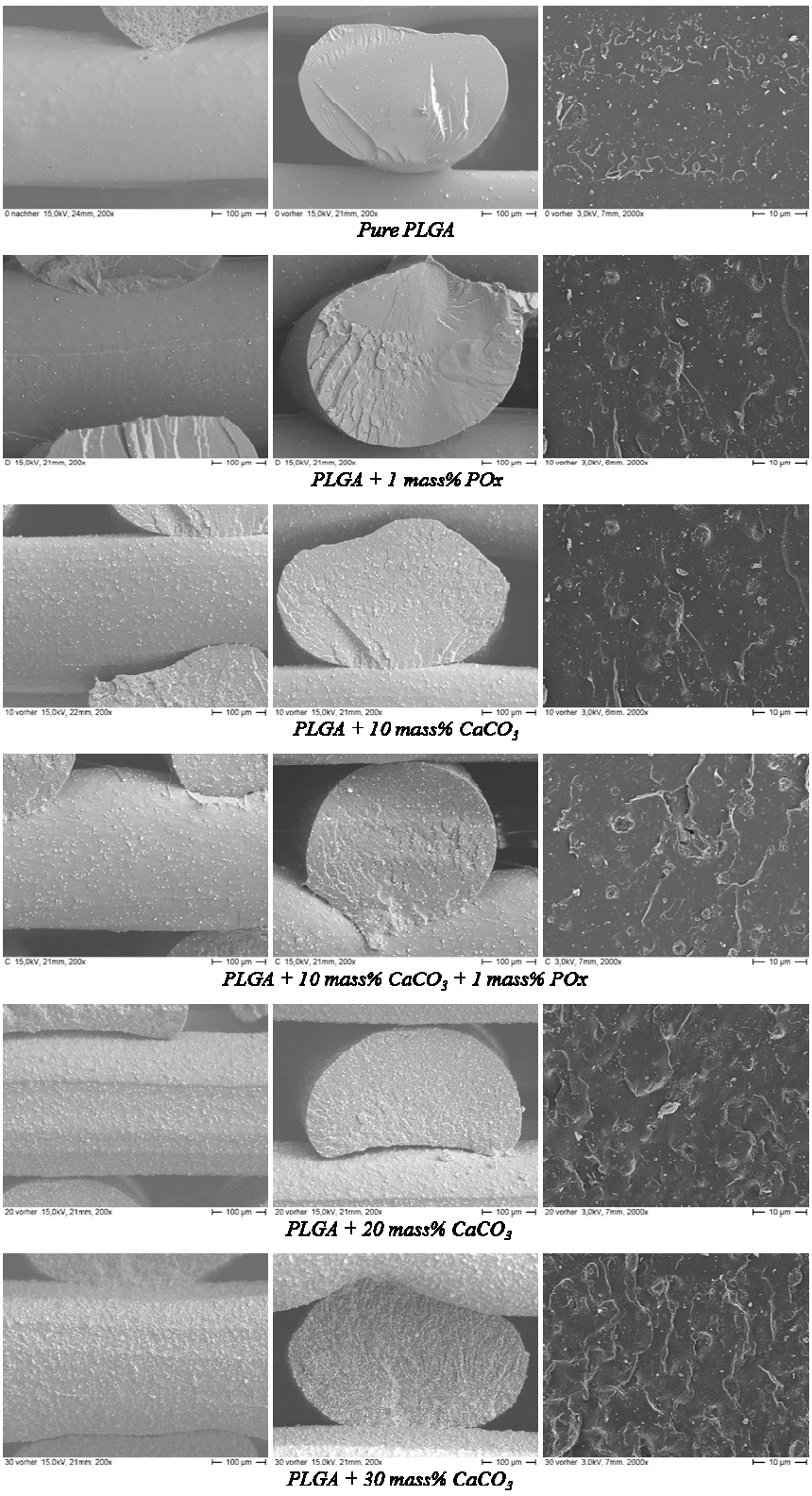

Fig. 7. SEM images of filament surfaces and filament cross sections (two different magnifications) for printed scaffolds from different melt systems (1st and 2nd column – 200×, 3rd column – 2000×)

more pronounced deviations in the diameter width. Thus, values for the filament thickness and its standard deviation changed from 350 ± 25.86 μm for pure PLGA to 470 ± 42.67 μm for PLGA + 30 mass % of $CaCO_3$.

The SEM images present a smooth filament surface for the PLGA and PLGA + 1 mass % of POx system. Addition of $CaCO_3$ results in an increasing roughness of the filament surface. The low magnifica-

tion cross section images display for the $CaCO_3$-containing systems a homogeneous distribution of the $CaCO_3$ particles and, in agreement, with Fig. 6, more flattened filaments for increasing $CaCO_3$ content. The high-magnification cross section images support the homogeneous distribution of the mineral particles and show their complete embedding within the polymer matrix. Additionally, both Pox-containing systems show some oval pore-like structures in the submicrometer range.

3.4. Surface wettability

The water contact angles of densely printed flat sample surfaces from four melt systems have been measured to study the effect of addition of $CaCO_3$ and POx on the wettability of the PLGA (Fig. 8). The highest contact angles were measured for pure PLGA (64.1 ± 2.7°). Both systems PLGA + 10 mass % of $CaCO_3$ and PLGA + 1 mass % of POx show significantly lower contact angles of 52.2 ± 2.9° and 49.7 ± 1.6°, respectively. The combination of both additives further reduces the contact angle to 43.0 ± 2.3°.

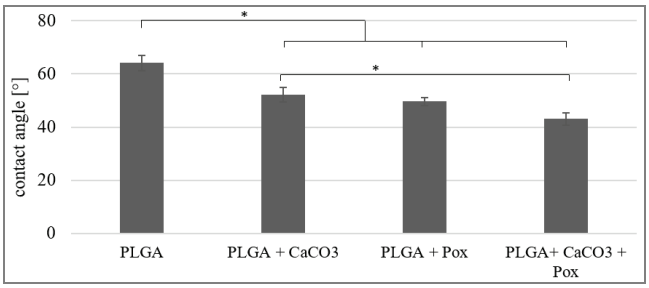

Fig. 8. Water contact angles on dense printed samples: PLGA, PLGA + 10 mass % of $CaCO_3$, PLGA + 1 mass % of POx, PLGA + 10 mass % of $CaCO_3$ + 1 mass % of POx

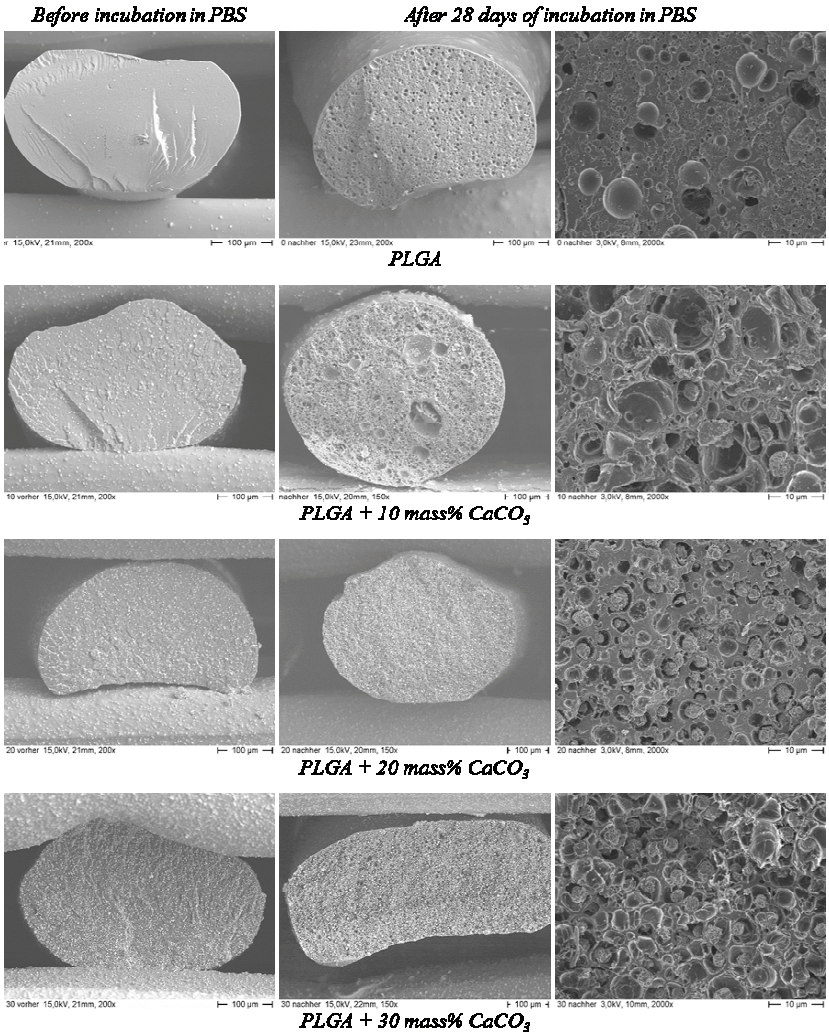

Fig. 9. SEM images of filament surfaces and filament cross sections (two different magnifications) for printed scaffolds from different melt systems prior and after 28 days incubation in PBS at 37 °C (1st and 2nd column – 200×, 3rd column – 2000×)

3.5. In vitro degradation behaviour in PBS

SEM investigations of the samples after incubation in PBS at 37 °C for 28 days show increasing inner porosity of the different scaffold compositions for increasing mineral content (Fig. 9), with only very few pores visible from the filament surface. For pure PLGA, three types of pores can be distinguished: (i) numerous bubble-like pores with a smooth inner surface in a diameter range between 2 and 6 μm, (ii) irregularly shaped pores in the same diameter range, and (iii) submicrometer pores throughout the sample. The samples with $CaCO_3$ show a markedly different porosity composed of cavities differing in size and containing mineral particles. Whereas these cavities range between 2 and 10 μm in diameter for the sample with 10 mass % of $CaCO_3$, an almost dense pattern of cavities with diameters between 2 and 4 μm dominates for the samples with 30 mass % of $CaCO_3$. For the 20 mass % of $CaCO_3$ sample, the general appearance is close to the 30 mass % sample, however with a lower degree of porosity, i.e., some dense PLGA matrix is still present.

Incubation in PBS resulted in changes in molecular weight and polydispersity. For example, M_n of PLGA in the scaffolds PLGA + 10 mass % of $CaCO_3$ prior to the experiment was 44.000 ± 460 g/mol and it decreased significantly to 36.000 ± 760 g/mol and 26.400 ± 790 g/mol after one week and 28 days, respectively. The dispersity decreased in this time frame from 4.8 ± 0.5 to 4.5 ± 0.2 and 4.2 ± 0.3, respectively.

4. Discussion

In biomaterials science, a key issue of current research is focussed on the improvement of the biological response of the damaged tissue and with that the healing success by tailoring the physico-chemical and biochemical biomaterials surface properties [10]. The goal of the presented work was to apply FDM printing to multi-component systems from PLGA, $CaCO_3$ and an amphiphilic polymer, and to study the bulk and surface properties of the resulting constructs as well as their *in vitro* degradation behavior. We aimed at using FDM processing to generate macro- and microporous geometries and to tailor the scaffold's surface topography and wetting behavior in a one step process. Our special interest was to study whether the combination of amphiphilic molecules and $CaCO_3$ results in a synergistic effect regarding the scaffold's wetting behavior.

4.1. Influence of printing parameters on scaffold geometry

As shown in Figs. 3 and 4, a variation of the printing parameters can be used to fine-tune the scaffold geometry with respect to filament width and pore size. The results demonstrate that an increase in printing head feed rate results in thinner strains and bigger pore size. On the other hand, an increase in extruder feed rate results in smaller pore size and thicker strains. Due to faster extruder rotations more material is released through the nozzle per time unit, which may, in combination with an increased printing head feed rate, enable a successful faster printing process as an alternative or in addition to multi-head printing systems [21]. Fine-tuning of the complex printing parameters set was however outside the focus of our work.

During printing an increase in the melt flow rate through the needle has been observed with a prolonged residence time in the tank for constant printing temperatures (T_t and T_e). As the material flow rate is connected with the melt viscosity, which depends on the molecular weight of PLGA, this is a clear indication of PLGA degradation during storage in the tank. This issue will be discussed in more detail in the paragraph 4.3.

4.2. Morphology of 3D scaffolds

Light microscopic observations reveal a decreasing transparency of the filaments for higher $CaCO_3$ contents in the melt system, while addition of POx results in a slightly brownish coloration, although thermal degradation of POx can be excluded under the given processing conditions [12]. Surprisingly, the addition of 20 and more mass % of $CaCO_3$ to the PLGA affects the final filament cross-section after printing under standard conditions indicating a lower viscosity of high mineral melts, compared to the respective melt systems with no added mineral. Additionally, SEM observations reveal an increasing filament surface roughness for higher $CaCO_3$ concentrations starting from smooth surfaces for PLGA and PLGA + 1 mass % of POx. However, SEM using high magnifications shows only mineral particles embedded in the surrounding polymer matrix and fully covered with a thin polymer coating for all $CaCO_3$-containing

melt systems. This is in agreement with Simpson et al. [22] who prepared PLGA/mineral matrix composites with ~45 mass % of mineral. After processing with either rudimentary injection moulding or compression moulding all mineral particles were completely embedded in the polymer matrix.

4.3. Molar mass evaluation

The working mechanism of the 3D printer used in this work is based on material melting inside the storage tank followed by transport to the printing needle by an extruder. Thus, material put to the tank is available for printing after a melting time of 10–12 min. Consequently, melt used for printing represents material exposed for different duration to the printing temperatures. Against this technological aspect, the decrease in the molecular mass of the polymer induced during the melting time and further exposure to elevated temperatures during the printing process has been investigated.

The observed strong decrease in the molecular weight during the melting time indicates an initial relatively fast random breakage of long polymer chains due to the thermal degradation [21]. This breakdown is probably caused by water residues present in the tank and on the surface of the starting materials. Such traces of water can result in an accelerated degradation of PLGA [7] and result for the given conditions in a decrease of the molecular weight to about one third of the starting value within the melting time. Results from a system PLGA + 10 mass % of $CaCO_3$ imply no effect of the mineral on the thermal PLGA degradation.

The ongoing thermal degradation of the PLGA during printing (up to ~120 min of printing) results in a further decrease of the PLGA's molecular weight to about one third of the value after the melting time. This decrease in the molecular weight is associated with a decrease in melt viscosity which would cause an increase of the melt stream through the printing needle with time under otherwise constant conditions. The easiest way to counteract and keep the melt stream constant under the given technological conditions is the continuous decrease of the printing temperatures, as indicated in Chapter 3.

In the work of Simpson et al. [22] thermal degradation for PLGA/mineral matrix composites has been followed for $CaCO_3$, hydroxyapatite and two types of bioglasses as mineral phase. Temperature time regimes between 51 s at 180 °C and 420 s at 220 °C resulted in a decrease of M_w between 20 and 95% depending both on the mineral phase and the temperature time regime. Similarly, Shim et al. [21] studied thermal degradation of pure PLGA in a multi-head deposition system for residence times up to 7 days at 120 °C. Whereas 1 day residence caused a reduction of M_w by more than 60%, longer duration produced in a more gradual breakdown of M_w down to 10% of the starting M_w after 7 days. Due to the markedly higher printing temperatures in our case, a similar breakdown within 2 h during the printing process is in good agreement with these findings.

4.4. Surface wettability

High hydrophobicity of PLGA scaffolds is an issue for many biological applications and diverse handling techniques have been developed to overcome this disadvantage [26]. The results of the water contact angle measurements displayed in Fig. 9 indicate significant positive effects both of the $CaCO_3$ and the POx content on the wetting behavior of printed constructs. For $CaCO_3$, the SEM investigations give no indications for uncovered mineral surface available for water contact. Thus, the effect of the mineral content must be traced back to the changes in the PLGA constructs surface topography, i.e., the wetting of micro-structured surfaces in the Wenzel regime [1]. Similar effects were discussed for etched titanium surfaces to improve both the wetting behavior and the biological response [19]. For Pox-containing systems, the surface topography was unchanged, compared to those with pure PLGA. Thus, a regio-selective self-organization of the POx molecules with the hydrophilic parts reaching outside the PLGA surface (surface segregation) during printing must be assumed as causation. This observation corresponds well with the improved wetting behavior of PLGA surfaces after surface hydrolysis via treatment with NaOH [3]. Similar effects have been observed for oxygen plasma treatment [17], [23] of PLGA. Thus, Wan et al. [23] report a decrease of water contact angles from 78° for the starting material to 45° after 2 minutes of plasma treatment. Both groups describe changes in the surface chemistry as well as the development of a sub µm surface topography during plasma treatment which is expected to contribute to the improved wetting behavior.

As shown in Fig. 8, the combination of $CaCO_3$ and POx content causes further significant decrease of the water contact angle, compared to pure PLGA and PLGA + 10 mass % of $CaCO_3$. Thus, a synergistic effect can be assumed that combines topographic

features from the mineral phase with chemical features of the self-organized arrangement of POx molecules in the PLGA/environment interface comparable to the investigations of Wan et al. [23]. The decrease in water contact angle to ~40° is expected to have a positive influence on the interaction with human cells as improved cell adhesion was shown for titanium surfaces with similar topography and wetting behaviour [19].

4.5. *In vitro* degradation in PBS

Storage of printed samples was performed in PBS at 37 °C for up to 28 days to study the hydrolytic *in vitro* degradation of selected samples. For pure PLGA, this resulted in the formation of a bimodal porosity with diameters of a few µm as well as in the submicrometer range. Addition of $CaCO_3$ changed porosity to a mineral particle-associated one. Pore distribution became more homogeneous along with increasing mineral content forming a dense pattern of cavities for the samples with initial content of 30 mass % of $CaCO_3$. In all cases, the outer shape of the filaments was completely maintained.

Exposure of porous scaffolds from PLGA70/30 and with 30 mass % tricalcium phosphate (TCP) prepared via solvent casting and porogen leaching in PBS for up to 12 weeks shows first micropores after 4 weeks of incubation [28]. For this approach, the obtained pores seemed not to be correlated with mineral particles which were very inhomogenously distributed within the scaffolds. SEM investigations of scaffolds' surfaces prepared by low-temperature printing of a slurry from PLGA70/30 and with 30 mass % TCP [27] show at numerous pores in the micrometer range after 12 weeks degradation in PBS at 37 °C. After 22 weeks a totally porous surface was observed. The authors did not provide cross-section images.

The reduction in M_w from 44.000 ± 460 g/mol to 26,400 ± 790 g/mol within 28 days incubation in PBS at 37 °C is in good agreement with data reported by Wu et al. [26] for porous scaffolds prepared by a room temperature approach from PLGA85/15, i.e., the polymer material systems used in our work. The authors found significantly faster degradation of PLGA75/25 scaffolds. A slower *in vitro* degradation has been detected by Yang et al. [27] for PLGA70/30 with 30 mass % TCP. Four weeks exposure in PBS at 37 °C reduced M_w only from 82.000 g/mol to 55.000 g/mol, indicating a decelerating effect of the mineral phase on PLGA degradation.

5. Conclusions

In this study, we demonstrated that FDM processing can be successfully applied to print three-dimensional scaffolds from three-component systems composed of PLGA, mineral and an amphiphilic polymer, resulting in a complete embedding and homogeneous distribution of the mineral particles in the polymer matrix. Printing conditions allowed for a regio-selective self-organization of the amphiphilic molecules in the PLGA surface with the hydrophilic parts reaching outside. Interestingly, the grouping of $CaCO_3$ and the amphiphilic polymer showed synergistic effects on the wettability behavior of the scaffolds. Our data emphasized that this behavior was due to a combination of surface topography with surface chemistry. Addition of $CaCO_3$ caused the further development of a mineral associated homogeneous micrometer-sized porosity during *in vitro* degradation. Together with the improved wetting behavior, this might enhance the biological response to our scaffolds prepared in a one-step processing. The observed significant thermal degradation of PLGA during scaffold fabrication might be overcome by printing technologies that allow for shorter high temperature material processing in the printing process.

Acknowledgements

The authors gratefully acknowledge financial support from the Federal Ministry of Education and Research, Germany (German-Polish project *GoBone*, No.01DS16010A) and AGH University of Science and Technology statutory founds (No. 11.11.160.182). Authors would also like to acknowledge Mrs. Sylvia Mühle, TU Dresden for assistance in the SEM investigations.

References

[1] BICO J., TORDEUX C., QUÉRÉ D., *Rough wetting*, Europhys. Lett., 2001, 55(2), 214–20.

[2] CHEN G., XIA Y., LU X., ZHOU X., ZHANG F., GU N., *Effects of surface functionalization of PLGA membranes for guided bone regeneration on proliferation and behavior of osteoblasts*, J. Biomed. Mater. Res. – Part A, 2013, 101 A(1), 44–53.

[3] CROLL T.I., O'CONNOR A.J., STEVENS G.W., COOPER-WHITE J.J., *Controllable surface modification of poly(lactic-co-glycolic acid) (PLGA) by hydrolysis or aminolysis I: Physical, chemical, and theoretical aspects*, Biomacromolecules, 2004, 5(2), 463–73.

[4] DHANDAYUTHAPANI B., YOSHIDA Y., MAEKAWA T., KUMAR D.S., *Polymeric scaffolds in tissue engineering application: A review*, Int. J. Polym. Sci., 2011(ii).

[5] DUAN B., WANG M., ZHOU W.Y., CHEUNG W.L., LI Z.Y., LU W.W., *Three-dimensional nanocomposite scaffolds fabricated via selective laser sintering for bone tissue engineering*, Acta Biomater., 2010, 6(12), 4495–4505.

[6] FLATH T., NEUNZEHN J., HACKER M.C., WIESMANN H.-P., SCHULZ-SIEGMUND, MICHAELA SCHULZE F.P., *Ein Doppelschneckenextruder zur Materialdosierung in einem Rapid Prototyping-Prozess*, 2016.

[7] HOUCHIN M.L., TOPP E.M., *Physical properties of PLGA films during polymer degradation*, J. Appl. Polym. Sci., 2009, 114(5), 2848–54.

[8] HUANG Y., REN J., REN T., GU S., TAN Q. et al., *Bone marrow stromal cells cultured on poly (lactide-co-glycolide)/ nano-hydroxyapatite composites with chemical immobilization of Arg-Gly-Asp peptide and preliminary bone regeneration of mandibular defect thereof*, J. Biomed. Mater. Res. – Part A, 2010, 95(4), 993–1003.

[9] IDASZEK J., BRUININK A., WIĘSZKOWSKI W., *Delayed degradation of poly(lactide-co-glycolide) accelerates hydrolysis of poly(ε-caprolactone) in ternary composite scaffolds*, Polym. Degrad. Stab., 2016, 124, 119–27.

[10] JUNKER R., DIMAKIS A., THONEICK M., JANSEN J.A., *Effects of implant surface coatings and composition on bone integration: A systematic review*, Clin. Oral. Implants Res., 2009, 20 (Suppl. 4), 185–206.

[11] KIM J., MCBRIDE S., TELLIS B., ALVAREZ-URENA P., SONG Y.H. et al., *Rapid-prototyped PLGA/β-TCP/hydroxyapatite nanocomposite scaffolds in a rabbit femoral defect model*, Biofabrication, 2012, 4(2).

[12] KOURTI M.E., FOTINOGIANNOPOULOU G., FEGA E., PITSIKALIS M., *Statistical Copolymers of 2-Methyl- and 2-Phenyl-oxazoline by Metallocene-Mediated Cationic Ring-Opening Polymerization: Synthesis, Reactivity Ratios, Kinetics of Thermal Decomposition and Self-Assembly Behavior in Aqueous Solutions*, J. Macromol. Sci. Part A Pure Appl. Chem., 2015, 52(8), 630–41.

[13] LEE J.W., KANG K.S., LEE S.H., KIM J.Y., LEE B.K., CHO D.W., *Bone regeneration using a microstereolithography-produced customized poly(propylene fumarate)/diethyl fumarate photopolymer 3D scaffold incorporating BMP-2 loaded PLGA microspheres*, Biomaterials, 2011, 32(3), 744–52.

[14] LI J., STAYSHICH R.M., MEYER T.Y., *Exploiting sequence to control the hydrolysis behavior of biodegradable PLGA copolymers*, J. Am. Chem. Soc., 2011, 133(18), 6910–13.

[15] METWALLY H.A., ARDAZISHVILI R.V., SEVERYUKHINA A.N., ZAHAREVICH A.M., SKAPTSOV A.A. et al., *The Influence of Hydroxyapatite and Calcium Carbonate Microparticles on the Mechanical Properties of Nonwoven Composite Materials Based on Polycaprolactone*, Bionanoscience, 2014, 5(1), 22–30.

[16] PARK S.H., PARK D.S., SHIN J.W., KANG Y.G., KIM H.K. et al., *Scaffolds for bone tissue engineering fabricated from two different materials by the rapid prototyping technique: PCL versus PLGA*, J. Mater. Sci. Mater. Med., 2012, 23(11), 2671–78.

[17] QU X., CUI W., YANG F., MIN C., SHEN H. et al., *The effect of oxygen plasma pretreatment and incubation in modified simulated body fluids on the formation of bone-like apatite on poly(lactide-co-glycolide) (70/30)*, Biomaterials, 2007, 28(1), 9–18.

[18] RUMIAN L., WOJAK I., SCHARNWEBER D., PAMULA E., *Resorbable scaffolds modified with collagen type I or hydroxyapatite: in vitro studies on human mesenchymal stem cells*, Acta Bioeng. Biomech., 2013, 15(1), 61–67.

[19] RUPP F., SCHEIDELER L., REHBEIN D., AXMANN D., GEIS--GERSTORFER J., *Roughness induced dynamic changes of wettability of acid etched titanium implant modifications*, Biomaterials, 2004, 25(7–8), 1429–38.

[20] SCHARNWEBER D., HUBNER L., ROTHER S., HEMPEL U., ANDEREGG U. et al., *Glycosaminoglycan derivatives: promising candidates for the design of functional biomaterials*, J. Mater. Sci. Med., 2015, 26(9).

[21] SHIM J.-H., KIM J.Y., LEE S.-H., KANG S.-W., *Effect of Thermal Degradation of SFF-Based PLGA Scaffolds Fabricated Using a Multi-head Deposition System Followed by Change of Cell Growth Rate*, J. Biomater. Sci., 2010, 1069–80.

[22] SIMPSON R.L., NAZHAT S.N., BLAKER J.J., BISMARCK A., HILL R. et al., *A comparative study of the effects of different bioactive fillers in PLGA matrix composites and their suitability as bone substitute materials: A thermo-mechanical and in vitro investigation*, J. Mech. Behav. Biomed. Mater., 2015, 50, 277–89.

[23] WAN Y., QU X., LU J., ZHU C., WAN L. et al., *Characterization of surface property of poly(lactide-co-glycolide) after oxygen plasma treatment*, Biomaterials, 2004, 25(19), 4777–4783.

[24] WOJAK-CWIK I.M., HINTZE V., SCHNABELRAUCH M., MOELLER S., DOBRZYŃSKI P. et al., *Poly(L-lactide-co-glycolide) scaffolds coated with collagen and glycosaminoglycans: Impact on proliferation and osteogenic differentiation of human mesenchymal stem cells*, J. Biomed. Mater. Res. Part A, 2013, 101(11), 3109–22.

[25] WOJAK I., PAMUŁA E., DOBRZYŃSKI P., ZIMMERMANN H., WORCH H. et al., *Coating of poly(l-lactide-co-glycolide) scaffolds with collagen/glycosaminoglycan matrices and their effects on osteoblast behaviour*, Eng. Biomater., 2009, 12, 9–13.

[26] WU L., DING J., *In vitro degradation of three-dimensional porous poly(D,L-lactide-co- glycolide) scaffolds for tissue engineering*, Biomaterials, 2004, 25(27), 5821–30.

[27] YANG F., CUI W., XIONG Z., LIU L., BEI J., WANG S., *Poly(l,l--lactide-co-glycolide)/tricalcium phosphate composite scaffold and its various changes during degradation in vitro*, Polym. Degrad. Stab., 2006, 91(12), 3065–73.

[28] YANG Y., ZHAO Y., TANG G., LI H., YUAN X., FAN Y., *In vitro degradation of porous poly(l-lactide-co-glycolide)/β--tricalcium phosphate (PLGA/β-TCP) scaffolds under dynamic and static conditions*, Polym. Degrad. Stab., 2008, 93(10), 1838–45.

[29] YEN H.J., TSENG C.S., HSU S.H., TSAI C.L., *Evaluation of chondrocyte growth in the highly porous scaffolds made by fused deposition manufacturing (FDM) filled with type II collagen*, Biomed. Microdevices, 2009, 11(3), 615–24.